Observation of Kondo hybridization with an orbital-selective Mott phase in 4*d* $Ca_{2-x}Sr_xRuO_4$

Minsoo Kim
Center for Correlated Electron Systems, Institute for Basic Science https://orcid.org/0000-0002-4137-4610

Junyoung Kwon
Center for Correlated Electron Systems, Institute for Basic Science

Choong H. Kim
Institute for Basic Science https://orcid.org/0000-0002-9149-1401

Daun Chung
Center for Correlated Electron Systems, Institute for Basic Science

Younsik Kim
Center for Correlated Electron Systems, Institute for Basic Science

Hanyoung Ryu
Institute for Basic Science

Jongkeun Jung
Center for Correlated Electron Systems, Institute for Basic Science

Beom Seo Kim
Seoul National University

Dongjoon Song
National Institute of Advanced Industrial Science and Technology

Jonathan Denlinger
Lawrence Berkeley National Lab

Moonsup Han
University of Seoul https://orcid.org/0000-0003-0993-040X

Yoshiyuki Yoshida
National Institute of Advanced Industrial Science and Technology (AIST)

Takashi Mizokawa
Waseda University https://orcid.org/0000-0002-7682-2348

Wonshik Kyung (specialtoss@gmail.com)
Center for Correlated Electron Systems, Institute for Basic Science

Changyoung Kim (changyoung@snu.ac.kr)
Seoul National University

Article

Keywords: Kondo-hybridization (KH), 4d/5d transition metal compounds, orbital-selective Mott phase (OSMP)

Posted Date: August 11th, 2020

DOI: https://doi.org/10.21203/rs.3.rs-48339/v1

Version of Record: A version of this preprint was published at npj Quantum Materials on June 8th, 2022. See the published version at https://doi.org/10.1038/s41535-022-00471-5.

Abstract

The heavy fermion state with Kondo-hybridization (KH), usually manifested in *f*-electron systems with lanthanide or actinide elements, was recently discovered in several 3*d* transition metal compounds without *f*-electrons. However, KH has not yet been observed in 4*d*/5*d* transition metal compounds, since more extended 4*d*/5*d* orbitals do not usually form flat bands that supply localized electrons appropriate for Kondo pairing. Here, we report a doping- and temperature-dependent angle-resolved photoemission study on 4*d* $Ca_{2-x}Sr_xRuO_4$, which shows the signature of KH. We observed a spectral weight transfer in the γ-band, reminiscent of an orbital-selective Mott phase (OSMP). The Mott localized γ-band induces the KH with an itinerant β-band, resulting in spectral weight suppression around the Fermi level. Our work is the first to demonstrate the evolution of the OSMP with possible KH among 4*d* electrons, and thereby expands the material boundary of Kondo physics to 4*d* multi-orbital systems.

Introduction

The heavy fermion (HF) state is one of the most important subjects in strongly correlated systems research and is often accompanied by exotic states such as superconductivity, quantum criticality and magnetism[1]. In early studies, HF behaviour was mostly found in *f*-electron systems in which strongly localized *f*- and itinerant *spd*- hybridized orbitals coexist and pair to form Kondo-singlets[2]. Recently, unexpected HF states have been discovered in moderately localized 3*d*-electron systems such as $CaCu_3Ir_4O_{12}$, AFe_2As_2 (A=K, Rb, Cs), and Fe_3GeTe_2[3-5], providing a strong impetus to search for possible Kondo-pairing even in less localized 4*d*/5*d*-electron systems.

$Ca_{2-x}Sr_xRuO_4$ (CSRO), a 4*d* transition metal oxide (TMO), is a good candidate for a HF state. Previous experimental studies[6-8] showed that CSRO possesses HF-like quasiparticle states, which suggests the existence of an orbital-selective Mott phase (OSMP). This led to several angle-resolved photo-emission spectroscopy (ARPES) studies that aimed to obtain direct evidence of the OSMP in CSRO[9-11], but controversy still remains even regarding the very existence of the OSMP. Part of the reason for the inconsistent conclusions arises from the fact that those studies were performed with limited points in the parameter space, such as doping concentration (*x*) and temperature (*T*).

In this letter, we provide our systematic *x*- ($0.2 \leq x \leq 0.5$) and *T*-dependent ARPES results on CSRO. With variation in doping and *T*, a gradual orbital-selective opening of the soft gap is observed in the γ ($4d_{xy}$)-band with spectral weight transfer from lower- to higher- binding energy (BE), suggesting the emergence of the OSMP. We also observed unexpected spectral weight suppression of the β ($4d_{xz/yz}$)-band (but not a), which we attribute to Kondo-hybridization (KH) between the localized γ- and itinerant β-bands, based on previous studies[4-8,12-16]. Our results show the coincidence between the emergence of the OSMP (and KH) and octahedral tilting distortion, implying that tilting is the key parameter triggering the observed phenomena. Our results not only provide direct evidence of the OSMP, but also constitute the first demonstration of possible KH in 4*d* orbitals.

Results

CSRO takes three crystalline forms in terms of RuO_2 octahedral distortions[17] (Supplementary Information 2 and 5): (I) no rotation or tilting ($1.5 \leq x \leq 2$, $I4/mmm$), (II) finite rotation without tilting ($0.5 \leq x < 1.5$, $I4_1/acd$), and (III) finite rotation and tilting ($0 \leq x < 0.5$, $Pbca$). The Fermi surface (FS) topology varies significantly depending on the type of distortion (Fig. 1). In Sr_2RuO_4 (I), four electrons ($4d^4$) in the t_{2g} orbitals make up three FS pockets (Fig. 1a). When octahedral rotation occurs (II), the FS becomes zone-folded due to the reduced BZ (Fig. 1b). Finally, in III with octahedral tilting, the β and γ FS pockets are selectively suppressed while the α-pocket remains robust as seen in Fig. 1c. This behaviour is reminiscent of the OSMP.

To scrutinize this OSMP-like phenomenon, we performed systematic ARPES studies as a function of x and T. Our x-dependent result ($0.2 \leq x \leq 0.5$) is presented in Figs. 2a-d. As x decreases from $x = 0.5$ to 0.2, gradual suppression of the spectral weight is observed near the Fermi level generating a soft gap[19], as shown in Fig. S2b (Supplementary Information 2). Interestingly, the soft gap opens only for the β- and γ-bands, while the α-band remains intact with variation in doping. A similar trend is also observed in the T-dependence data (Figs. 2d, e-g). As T decreases from 45 K, the spectral weight of the β- and γ-bands is suppressed in a similar fashion to that observed for the doping dependent result.

A detailed analysis of the phenomena in Fig. 2 is provided in Fig. 3. It can clearly be seen in the momentum distribution curves (MDCs) for each x (Fig. 3a) that the β- and γ-bands are selectively suppressed as a function of x. The Lorentzian-fitted peak areas are plotted in Figs. 3b (x-dependent) and 3c (T-dependent), showing clear suppression only for the β- and γ-bands. The energy distribution curves (EDCs) in Fig. 3d also show the evolution of the soft gap in the γ-band as a function of T. As T decreases from 45 K, the spectral weight in the 'A' region (BE < 0.2 eV) is gradually suppressed, while it increases in the 'B' region (BE ~ 0.4 eV). Hence, the spectral weight is transferred from lower to higher BE. This behaviour can be seen more clearly in Fig. 3e, which shows the EDCs with the data obtained at 45 K subtracted. The integrated areas in the A and B regions are found to be almost identical, but with the opposite sign, satisfying the sum rule at all T (Fig. 3f). This suggests that the T-dependent evolution originates from spectral weight transfer rather than a T-driven spectral broadening effect[20]. Furthermore, the suppressed spectral weight is recovered upon small electron doping (Supplementary Information 6), which strongly suggests that the spectral weight suppression originates from Mott localization[21].

Discussion

Our observations (orbital-selective suppression and spectral weight transfer in the γ-band) are consistent with previously reported results on OSMP[10]. However, there are still questions to be resolved: for example, what triggers OSMP and why is the β-band suppressed in the same way as the γ-band. Previous experimental/theoretical studies suggested that octahedral rotation is responsible for the OSMP[10,22]. One study suggested that the rotation sufficiently reduces the γ-band width for Mott localization[22], and the

importance of $\sqrt{2} \times \sqrt{2} \times 2$ unit cell doubling due to the rotation has also been discussed[10]. In both scenarios, octahedral rotation plays a significant role in OSMP; thus, a larger rotation angle may lead to a stronger OSMP effect. However, the OSMP occurs after the octahedral rotation angle saturates to the maximum value at x=0.5. Our results show that the OSMP has the appearance of octahedral tilting distortion, and that the strength of the OSMP (spectral weight suppression of the γ-band) is roughly proportional to the tilting angle[17,22]. Therefore, even though octahedral rotation significantly reduces the bandwidth of the γ-band, the OSMP in CSRO is in fact triggered by octahedral tilting and not rotation.

The mechanism by which tilting triggers the OSMP can be understood by reference to the bandwidth change in each conduction band (Supplementary Information 5). As suggested in previous reports, octahedral rotation hybridizes d_{xy} and d_{x2-y2} orbitals, leading to bandwidth reduction in the γ-band[21]. In addition, at $x < 0.5$, octahedral tilting hybridizes the γ and d_{yz}/ d_{zx}(α-, β-bands), resulting in additional bandwidth reduction of the γ-band. In short, octahedral tilting further reduces the bandwidth to a sufficient degree to trigger the OSMP.
It is important to understand why the β-band is suppressed simultaneously with the OSMP. Since the OSMP occurs in the γ-band, Mott-localization in the β-band may be expected to occur in a similar fashion to that in the γ-band. However, while the electron occupation number of the γ-band ($n_\gamma \sim 1.5$)is appropriate for Mott localization in a doubled unit cell[10] (Supplementary Information 7), the electron numbers of the α- ($n_\alpha \sim 1.8$) and β- ($n_\beta \sim 0.7$) bands are inappropriate for Mott localization[9,10]. Therefore, a mechanism other than Mott localization is needed to explain the suppression of the β-band.We can gain insight into the origin of β-band suppression from previous studies[4,6-8,15,16]. Some experimental results on 3d iron-based superconductors (IBS) suggest that the emergence of OSMP leads to KH between itinerant (d_{yz}/ d_{zx}) and localized (d_{xy}) bands[4,15,16]. Interestingly, CSRO ($0.2 \leq x < 0.5$) exhibits the OSMP (similar to IBS), as well as HF-like behavior[6-8]; thus, the KH mechanism should be considered.

As seen in Figs. 4a and 4b, the β-band dispersion is significantly renormalized in a similar way to KH, as schematically illustrated in Figs. 4c and 4d. Here, the OSMP-driven localized γ-band plays the role of the localized band in KH, and the β-band provides itinerant electrons. Therefore, as the OSMP is strengthened from x = 0.5 to x = 0.2, the β-band is renormalized to β´ via KH with the γ-band. In this way, as shown in Fig. 2, the OSMP and KH vary simultaneously with changes in doping and T. Thus, suppression of the β-band can be understood as a result of incoherent-to-coherent crossover due to KH[24,25]. Our FS and Fermi momentum data (Figs. 1 and 4) also support the KH scenario. The β-band FS is reduced with OSMP (Figs. 4f and 4g) and the electron occupancy (n) of the β-band decreases from 0.72 (x = 0.5) to 0.63 (x = 0.2) with OSMP.

Furthermore, our ARPES results reveal that the β- and γ-bands are hybridized at temperatures lower than40 K (see Fig. 3d). Considering the logarithmic temperature dependence of Kondo effects, this temperature (< 40 K) is of a similar order to the incoherent-to-coherent crossover temperature T^*(14 K for x = 0.2) for resistivity[6,8,26] and the antiferromagnetic peak temperature T_p(12 K for x = 0.2) for magnetic susceptibility[8,26] (Supplementary Information 4). Therefore, hybridization between the β- and γ-

bands is likely due to KH which usually accompanies both incoherent-to-coherent crossover and antiferromagnetic states. Moreover, the theoretically estimated T_K value is in agreement with our experimentally observed value. HF systems exhibit scaling behaviour with respect to T_K which is given as[5]

$$\gamma_S \approx \frac{Rlog2}{T_K} \approx \frac{10,000}{T_K}\ [mJ/(\mathrm{K}^2 \cdot \mathrm{mol})], \quad (1)$$

where Y_s and R are the Sommerfeld coefficient and gas constant, respectively. The Y_s value is about 200-250 $mJ/$(K·mol) for CSRO ($0.2 \leq x \leq 0.5$)[7] and thus the estimated T_K is about 40-50 K, which is consistent with our experimentally estimated value (40 K). In this regard, the β-band suppression is likely due to KH between γ-(localized) and β-(itinerant) bands.

Then, the next question is why only the β-band is involved in KH, while the α-band remains unaffected. This phenomenon can be understood by reference to momentum-dependent-interaction theory, which is essential for explaining ferromagnetic-Kondo systems[25,27-30]. In that theory, the proximity of two bands in momentum space is one of the most important factors leading to interactions between them. As can be seen in Fig. 2, the β- and γ- bands are located close in momentum space. Therefore, KH can occur more easily than with the α-band, as illustrated in Fig. 4d.

Our work has important implications for aspects of both Mott and Kondo physics. Although CSRO was the first candidate proposed for demonstrating the OSMP, the existence of the OSMP in CSRO has not yet been universally agreed[10,11]. Our systematic *x*- and *T*- dependent studies not only settle this issue by demonstrating the gradual evolution of the OSMP but also provide clues to the microscopic mechanism of the OSMP by demonstrating the coincidence between octahedral tilting and the OSMP. Furthermore, this is the first to address KH among 4*d* orbitals. The OSMP-driven localized band enables KH with other itinerant 4*d* bands. Our work advances understanding of OSMP and Kondo physics in 4*d* TMOs, and suggests a key role for octahedral tilting in layered perovskite as a control parameter of physical properties.

Methods

- **Crystal growth and characterization**: High quality $Ca_{2-x}Sr_xRuO_4$ (x = 0.2, 0.3, 0.4, 0.5, 1.0, 2.0) were grown using the optical floating zone method. Sample quality and stoichiometry were characterized using a physical property measurement system (PPMS), a magnetic property measurement system (MPMS), scanning electron microscopy with energy dispersive X-ray analysis (SEM-EDX), and X-ray diffractometry.

- **Angle-resolved photoemission spectroscopy (ARPES)**: Temperature-dependent ARPES (hv = 70 eV) measurements were performed at MERLIN beam line 4.0.3 of the Advanced Light Source, Lawrence Berkeley National Laboratory using both LH (π) and LV (σ) polarizations from an elliptically polarized undulator. Spectra were acquired with an R8000 (BL 4.0.3) electron analyser. Cleaving of the samples was conducted at 10 K in an ultra-high vacuum better than 5×10^{-11} Torr.

Declarations

ACKNOWLEDGEMENTS

This work was supported by the Institute for Basic Science in Korea (Grant No. IBS-R009-G2). The English in this document has been checked by at least two professional editors, both native speakers of English. For a certificate, please see: http://www.textcheck.com/certificate/c9FWEt

AUTHOR CONTRIBUTIONS

M.K. and W.K. conceived the work. M.K., W.K., Y.K., H.R., J.J. and B.S.K. performed ARPES measurements with the support from J.D.D., and M. K. and D. C. analysed the data. Samples were grown and characterized by M.S.K., J.Y.K. and D.J.S., with support from Y.Y.. Theoretical studies and density functional theory calculations were performed by C.H.K.. All authors discussed the results. W.K. and C.K. led the project and manuscript preparation with contributions from all authors. Additional information, correspondence and requests for materials should be addressed to W. Kyung (specialtoss@gmail.com) and C. Kim (changyoung@snu.ac.kr)

COMPETING INTERESTS

We declare that we have no competing interests.

References

1. Stewart, S. G. Heavy-fermion systems. *Rev. Mod. Phys.* **56.4**, 755–787 (1984).
2. Jullien, R., Fields, J., & Doniach, S. Kondo lattice: Real-space renormalization-group approach. *Phys. Rev. Lett.* **38.25**, 1500–1503 (1977).
3. Cheng, J. G. et al. Possible Kondo physics near a metal-insulator crossover in the A-site ordered perovskite $CaCu_3Ir_4O_{12}$. *Phys. Rev. Lett.* **111.17**, 176403 (2013).
4. Wu, Y. P. et al. Emergent Kondo lattice behavior in iron-based superconductors AFe_2As_2 (A = K, Rb, Cs). *Phys. Rev. Lett.* **116.14**, 147001 (2016).
5. Zhang, Y. et al. Emergence of Kondo lattice behavior in a van der Waals itinerant ferromagnet, Fe_3GeTe_2. *Sci. Adv.* **4.1**, eaao6791 (2018).
6. Nakatsuji, S., & Maeno, Y. Quasi-two-dimensional Mott transition system $Ca_{2-x}Sr_xRuO_4$. *Phys. Rev. Lett.* **84.12**, 2666–2669 (2000).
7. Nakatsuji, S. et al. Heavy-mass Fermi liquid near a ferromagnetic instability in layered ruthenates. *Phys. Rev. Lett.* **90.13**, 137202 (2003).
8. Jin, R. et al. Heavy-electron behavior and structural change in $Ca_{1.7}Sr_{0.3}RuO_4$. Preprint at http://arXiv.org/abs/cond-mat/0112405 (2001).

9. Wang, S. C. et al. Fermi surface topology of $Ca_{1.5}Sr_{0.5}RuO_4$ determined by angle-resolved photoelectron spectroscopy. *Phys. Rev. Lett.* **93.17**, 177007 (2004).
10. Neupane, M. et al. Observation of a novel orbital selective Mott transition in $Ca_{1.8}Sr_{0.2}RuO_4$. *Phys. Rev. Lett.* **103.9**, 097001 (2009).
11. Shimoyamada, A. et al. Strong mass renormalization at a local momentum space in multiorbital $Ca_{1.8}Sr_{0.2}RuO_4$. *Phys. Rev. Lett.* **102.8**, 086401 (2009).
12. De Leo, L., Civelli, M., & Kotliar, G. T = 0 heavy-fermion quantum critical point as an orbital-selective Mott transition. *Phys. Rev. Lett.* **101.25**, 256404 (2008).
13. Denlinger, J. D. et al. Temperature dependence of linked gap and surface state evolution in the mixed valent topological insulator SmB_6. Preprint at http://arXiv.org/abs/1312.6637 (2013).
14. Frantzeskakis, E. et al. Kondo hybridization and the origin of metallic states at the (001) surface of SmB_6. *Phys. Rev. X* **3.4**, 041024 (2013).
15. Zhao, D. et al. Breakdown of single spin-fluid model in the heavily hole-doped superconductor $CsFe_2As_2$. *Phys. Rev. B* **97.4**, 045118 (2018).
16. Yi, M. et al. Observation of universal strong orbital-dependent correlation effects in iron chalcogenides. *Nat. commun.* **6.1**, 1–7 (2015).
17. Friedt, O. et al. Structural and magnetic aspects of the metal-insulator transition in $Ca_{2-x}Sr_xRuO_4$. *Phys. Rev. B* **63.17**, 174432 (2001).
18. Zhang, P. et al. A precise method for visualizing dispersive features in image plots. *Rev. Sci. Instrum.* **82.4**, 043712 (2011).
19. Kim, S. Y. et al. Spectroscopic studies on the metal–insulator transition mechanism in correlated materials. *Adv. Mater.* **30.42**, 1704777 (2018).
20. Sutter, D. et al. Orbitally selective breakdown of Fermi liquid quasiparticles in $Ca_{1.8}Sr_{0.2}RuO_4$. *Phys. Rev. B* **99.12**, 121115 (2019).
21. De La Torre, A. et al. Collapse of the Mott gap and emergence of a nodal liquid in lightly doped Sr_2IrO_4. *Phys. Rev. Lett.* **115.17**, 176402 (2015).
22. Ko, E., Kim, B. J., Kim, C., & Choi, H. J. Strong orbital-dependent *d*-band hybridization and Fermi-surface reconstruction in metallic $Ca_{2-x}Sr_xRuO_4$. *Phys. Rev. Lett.* **98.22**, 226401 (2007).
23. Noh, H. J. et al. Electronic structure and evolution of the orbital state in metallic $Ca_{2-x}Sr_xRuO_4$. *Phys. Rev. B* **72.5**, 052411 (2005).
24. Kummer, K. et al. Temperature-independent Fermi surface in the Kondo lattice $YbRh_2Si_2$. *Phys. Rev. X* **5.1**, 011028 (2015).
25. Jang, S. et al. Direct visualization of coexisting channels of interaction in CeSb. *Sci. Adv.* **5.3**, eaat7158 (2019).
26. Nakatsuji, S., and Maeno, Y. Switching of magnetic coupling by a structural symmetry change near the Mott transition in $Ca_{2-x}Sr_xRuO_4$. *Phys. Rev. B* **62.10**, 6458–6466 (2000).

27. Pruschke, T., Bulla, R., & Jarrell, M. Low-energy scale of the periodic Anderson model. *Phys. Rev. B* **61.19**, 12799–12809 (2000).
28. Liu, Y., Zhang, G. M., & Yu, L. Weak ferromagnetism with the Kondo screening effect in the Kondo lattice systems. *Phys. Rev. B* **87.13**, 134409 (2013).
29. Peters, R., Kawakami, N., & Pruschke, T. Spin-selective Kondo insulator: Cooperation of ferromagnetism and the Kondo effect. *Phys. Rev. Lett.* **108.8**, 086402 (2012).
30. Golež, D. Lifshitz phase transitions in the ferromagnetic regime of the Kondo lattice model. *Phys. Rev. B* **88.5**, 054431 (2013).

Figures

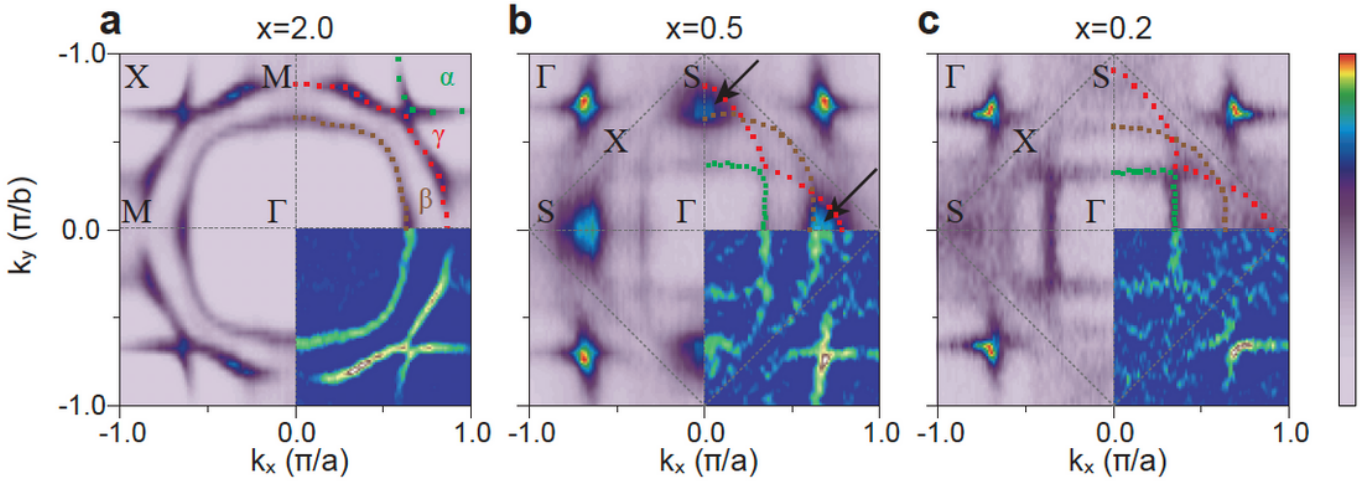

Figure 1

Fermi surfaces of Ca2-xSrxRuO4. (a-c) Fermi surfaces (FSs) of x = 2.0 (a), 0.5 (b), 0.2 (c) measured using angle-resolved photoemission spectroscopy (ARPES) at T = 10 K with π-polarized light. Color-coded dots indicate the Lorentzian-fitted peak positions of α (green), β (brown) and γ (red) FS pockets obtained from momentum distribution curves (MDCs). Grey dashed lines indicate the reduced Brillouin zone (BZ) due to octahedral distortions. High-symmetry points in the corresponding symmetry are marked for each doping condition. The right lower part of each panel shows a 2D curvature plot18 of the FS map.

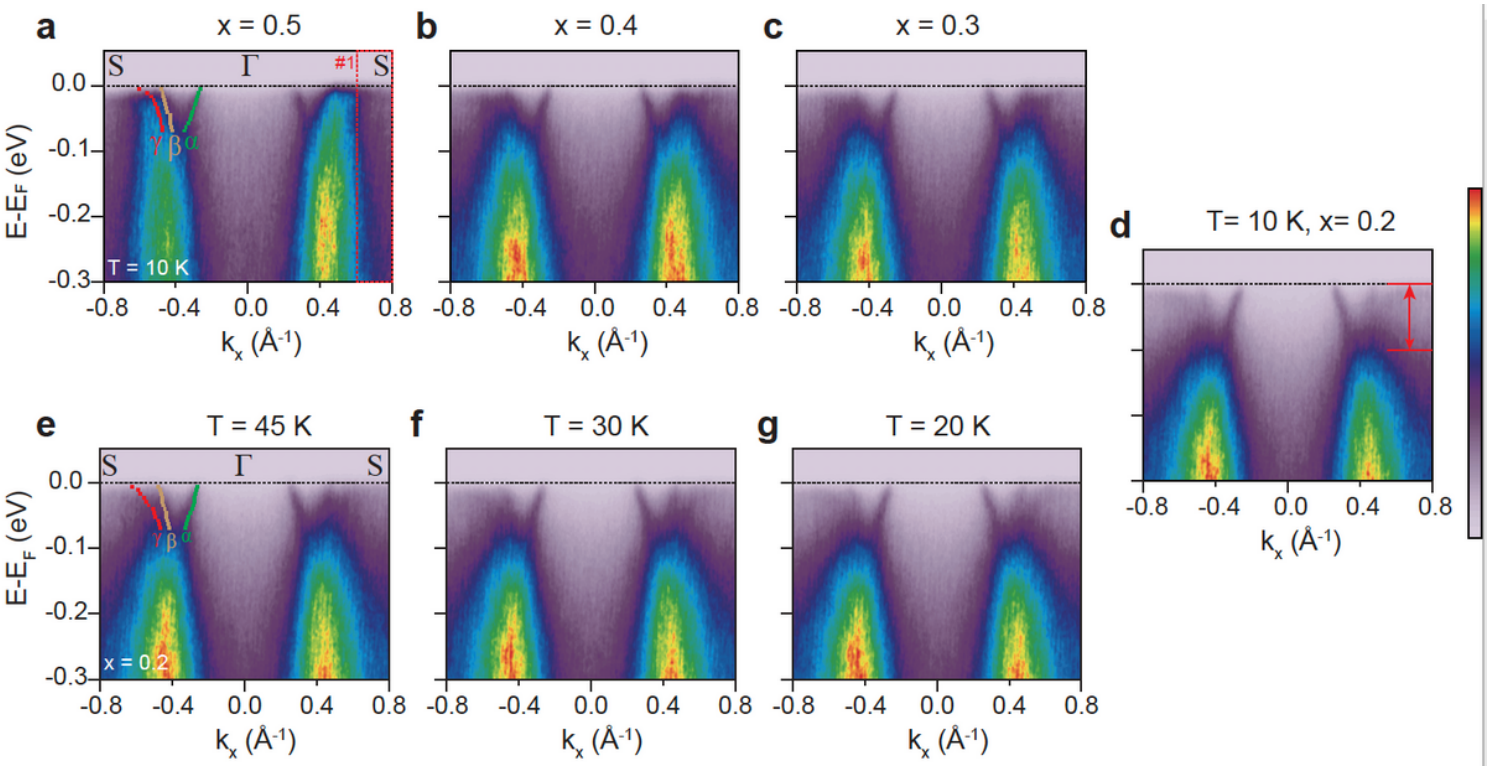

Figure 2

Doping- (x-) and temperature- (T-) dependent electronic structure evolution. (a-d) ARPES images along S-Γ-S for x = (a) 0.5, (b) 0.4, (c) 0.3, and (d) 0.2 measured at T = 10 K with π-polarized light. (d-g) ARPES data of x = 0.2 along S-Γ-S measured at T = (e) 45, (f) 30, (g) 20, and (d) 10 K. The red arrow in (d) indicates the region where the spectral weight was suppressed compared to (a) and (e).

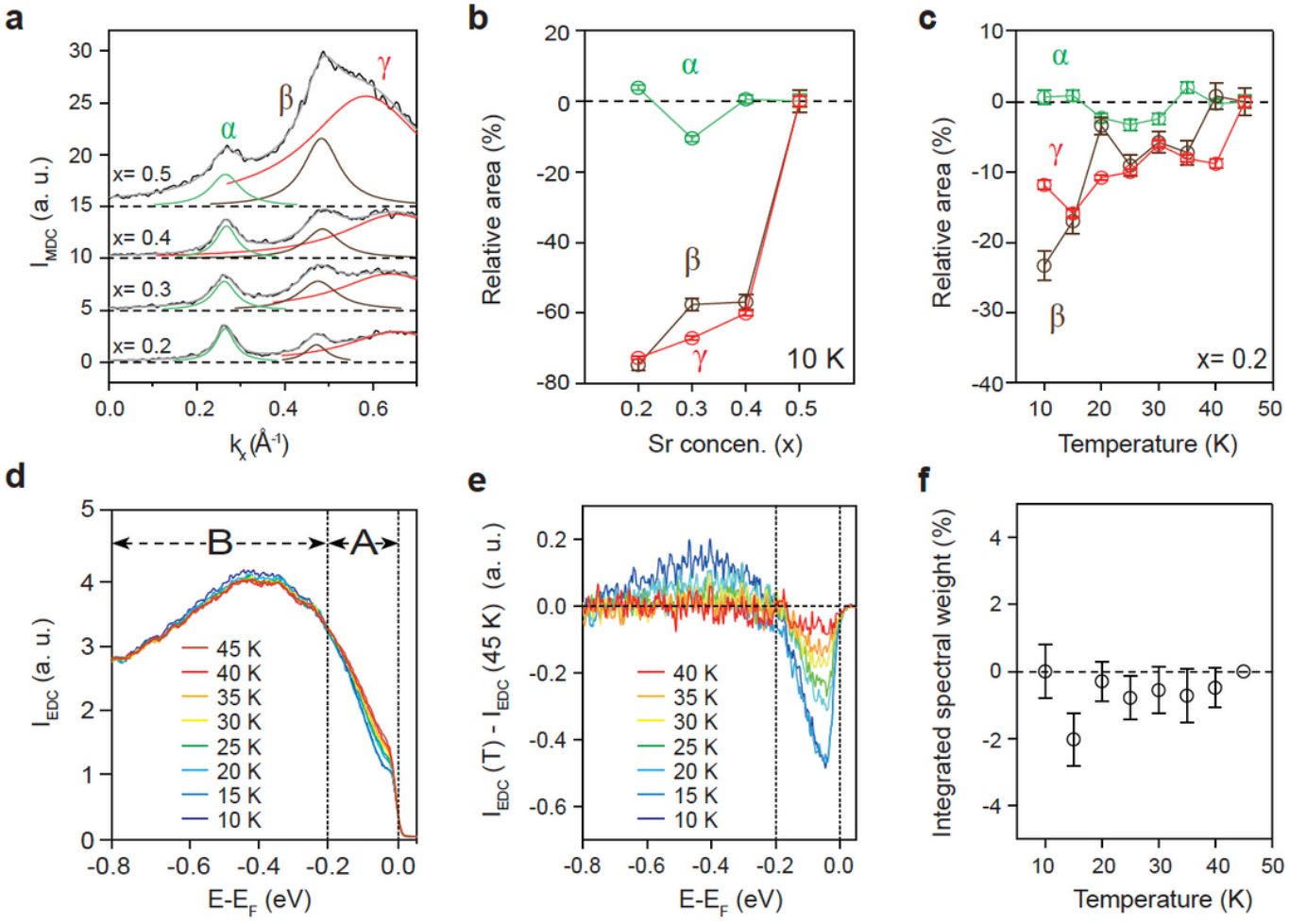

Figure 3

Band-selective suppression and spectral weight transfer. (a, b) Sr concentration (x)-dependent (a) normalized momentum distribution curves (MDCs) at the Fermi level (EF ±10 meV) along S-Γ-S. The solid coloured lines are Lorentzian fits (green: α, brown: β, red: γ). (b) x-dependent relative change in the Lorentzian fit area in (a) compared to that of x = 0.5. (c) T-dependent relative change in the Lorentzian fit area from the T-dependent MDCs (see Supplementary Information 3) compared to that at T = 45 K. (d) T-dependent integrated energy distribution curve (EDC) from region #2 in Fig. 2e and (e) with the EDC at 45 K subtracted. (f) Integrated EDC area (relative to the total integrated area of 45 K in (d)) in the region -0.8 < E-EF (eV) < 0.0 from (e) for each T. The zero values at each T suggest spectral weight conservation, implying the spectral weight transfer from low- to high-binding energy. A detailed explanation of the normalization method is provided in Supplementary Information 1.

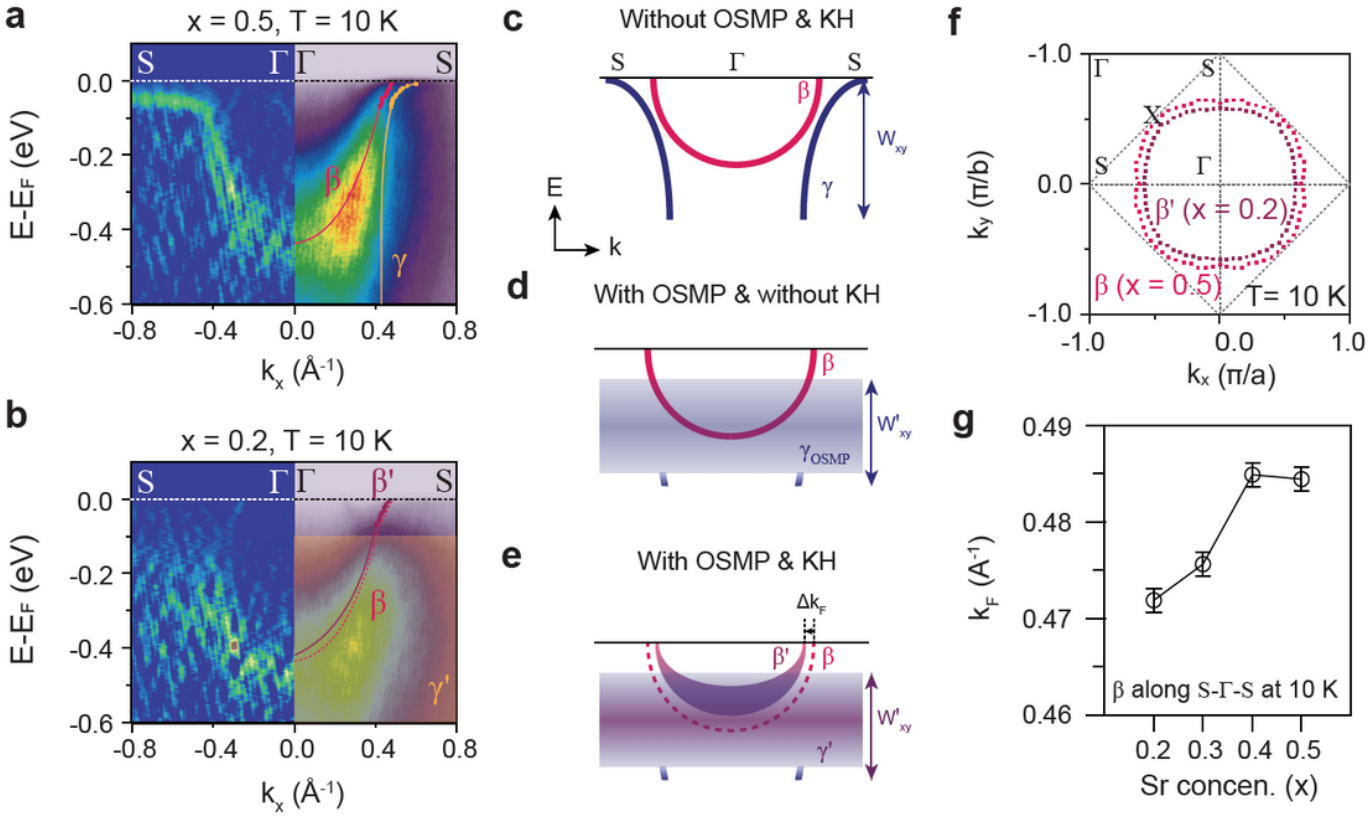

Figure 4

Kondo-hybridization (KH) among 4d t2g orbitals. (a, b) ARPES images (right) and corresponding 2D curvature plots18 (left) along S-Γ-S for x = (a) 0.5 and (b) 0.2 measured at T = 10 K with σ-polarized light. The solid-coloured lines overlaid on (a) and (b) denote the guidelines for each band (red: β-band, yellow: γ-band) extracted from Fig. 2; the purple line in (b) denotes the β' renormalized according to KH. The yellow shaded area in (b) indicates the Mott localized γ-band (γ'). (c-e) Schematic diagrams illustrating the evolution of the β- and γ-bands in three different cases: (c) without orbital-selective Mott phase (OSMP) and KH, (d) with OSMP and without KH and (e) with OSMP and KH. The γ-band dispersion is taken from the data in Fig. 2 which was obtained with π-polarized light. (f) Angle dependent Fermi momentum (kF) without- (x = 0.5, β) and with- (x = 0.2, β') KH extracted from Fig. 1. (g) Doping-dependent kF of the β-band extracted from Fig. 3a.

Supplementary Files

This is a list of supplementary files associated with this preprint. Click to download.

- draftSI.pdf